Nitric oxide prevents a pathogen permissive granulocytic inflammation during tuberculosis

Bibhuti B. Mishra[1], Rustin Lovewell[1], Andrew J Olive[1], Guoliang Zhang[3], Wenfei Wang[3], Eliseo Eugenin[4], Clare M Smith[1], Jia Phuah Yao[1], Jarukit E Long[1], Michelle L Dubuke[6], Samantha Palace[1], Jon D. Goguen[1], Richard Baker[1], Subhalaxmi Nambi[1], Rabinarayan Mishra[2], Matthew G Booty[1], Christina Baer[1], Scott A Shaffer[6], Veronique Dartois[4], Beth McCormick[1], Xinchun Chen[3,5]*, and Christopher M. Sassetti[1]*

[1] Department of Microbiology and Physiological Systems, University of Massachusetts Medical School. Worcester, MA. USA

[2] Department of Pathology, University of Massachusetts Medical School, Worcester, MA.USA

[3] Guangdong Key Lab of Emerging Infectious Diseases, Shenzhen Third People's Hospital, Guangdong Medical College, Shenzhen, 518112, China

[4] Public Health Research Institute Center at the International Center for Public Health New Jersey Medical School - Rutgers, New Jersey, USA

[5] Department of Pathogen Biology, Shenzhen University School of Medicine, Shenzhen 518060, China

[6] Proteomics and Mass Spectrometry Facility, Department of Biochemistry and Molecular Pharmacology, University of Massachusetts Medical School, Worcester, MA. USA.

Table of Contents:

Supplementary Figure 1. Loss of Nos2 results in increased IL-1 production and neutrophil influx

Supplementary Figure 2. Mice maintain chimerism after bone marrow reconstitution, and purified cells are representative of the total population.

Supplementary Figure 3. Specificity of neutrophil depletion methods.

Supplementary Figure 4. Neutrophils do not kill Mtb *ex vivo*.

Supplementary Figure 5. Effect of Nos2 and Nlrp3 and Il1r1 inhibition on gene expression

Supplementary Figure 6. 12/15-LOX has a larger effect on TB disease than 5-LOX or LTB4R1.

Supplementary Figure 7. 5- and 12/15-LOX products in the lung correlate with the extent of inflammation.

Supplementary Figure 8. Nonspecific antibodies do not stain human lung sections.

Supplementary Figure 9. Model to describe the role of pro- and anti-inflammatory pathways in TB pathogenesis.

Supplementary Figure 1:

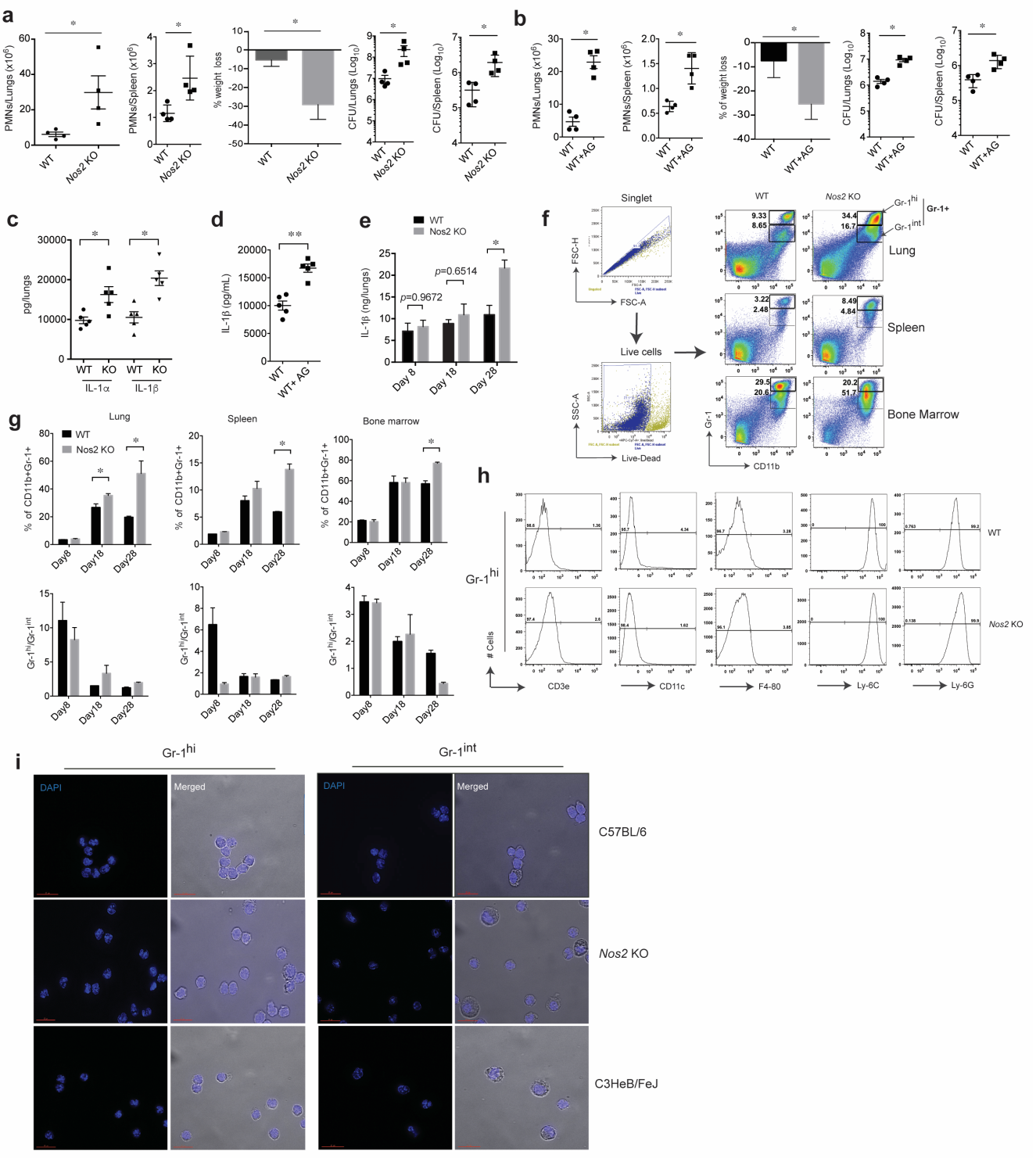

Supplementary Figure 1. Loss of Nos2 results in increased IL-1 production and sustained neutrophil influx

a. *Nos2*$^{-/-}$ mice were infected with Mtb. Four weeks' post infection, neutrophil numbers were determined by flow cytometry, % weight loss was determined relative to the beginning of infection, and bacterial load was assessed in the lung and spleen homogenates by CFU measurement. **b**. At five wks post infection, AG treated wild type C57BL/6J (WT) mice were analyzed for disease as in "a**"**. IL-1α and IL-1β were measured in the lung homogenates of (**c**) WT and *Nos2*$^{-/-}$ mice; (**d**) AG treated WT mice four weeks post infection, (**e**) WT and *Nos2*$^{-/-}$ mice at indicated time points post infection. (**a, b** and **d**), Values shown (Mean ± SD) representative of two independent experiments. (*, indicates $p<0.05$, two-tailed unpaired *t*-test with Welch correction). (**d** and **e**). Data shown (Mean ± SD) are representative of two independent experiments, *, $p<0.05$; **, $p<0.001$, one-way ANOVA with Tukey's multiple comparison test. Wild type and *Nos2*$^{-/-}$ mice were infected with Mtb, lungs, spleen and bone marrow were collected at indicated time points post infection, and the % of CD11b+Gr-1+ cells in the total live leukocytes in these organs was determined by flow cytometry. **f**. Representative FACS plots demonstrating that CD11b+Gr-1^{hi} cells preferentially accumulate in *Nos2*$^{-/-}$ mice at day 28 post infection. **g**. The percent of CD11b+Gr-1+ cells in different organs over time (top panel) and relative abundance of Gr-1^{hi} and Gr-1^{int} leukocytes in these organs were determined (bottom panel). *, $p<0.05$, one-way ANOVA with Tukey's multiple comparison test**. h**. CD11b+ Gr-1^{hi} cells from the lungs of WT and *Nos2*$^{-/-}$ mice were further phenotyped for the indicated leukocyte markers. (**f**-**h**). Data shown are from one experiment representative of two. **i**. FACS sorted Gr-1^{high} and Gr-1^{int} cells from the infected lungs of C57BL/6, Nos2 KO and C3HeB/FeJ mice were centrifuged onto cytoslides and stained with DAPI for analyzing nuclear morphology (Scale bar represents 15μm). Data shown are from one experiment.

Supplementary Figure 2:

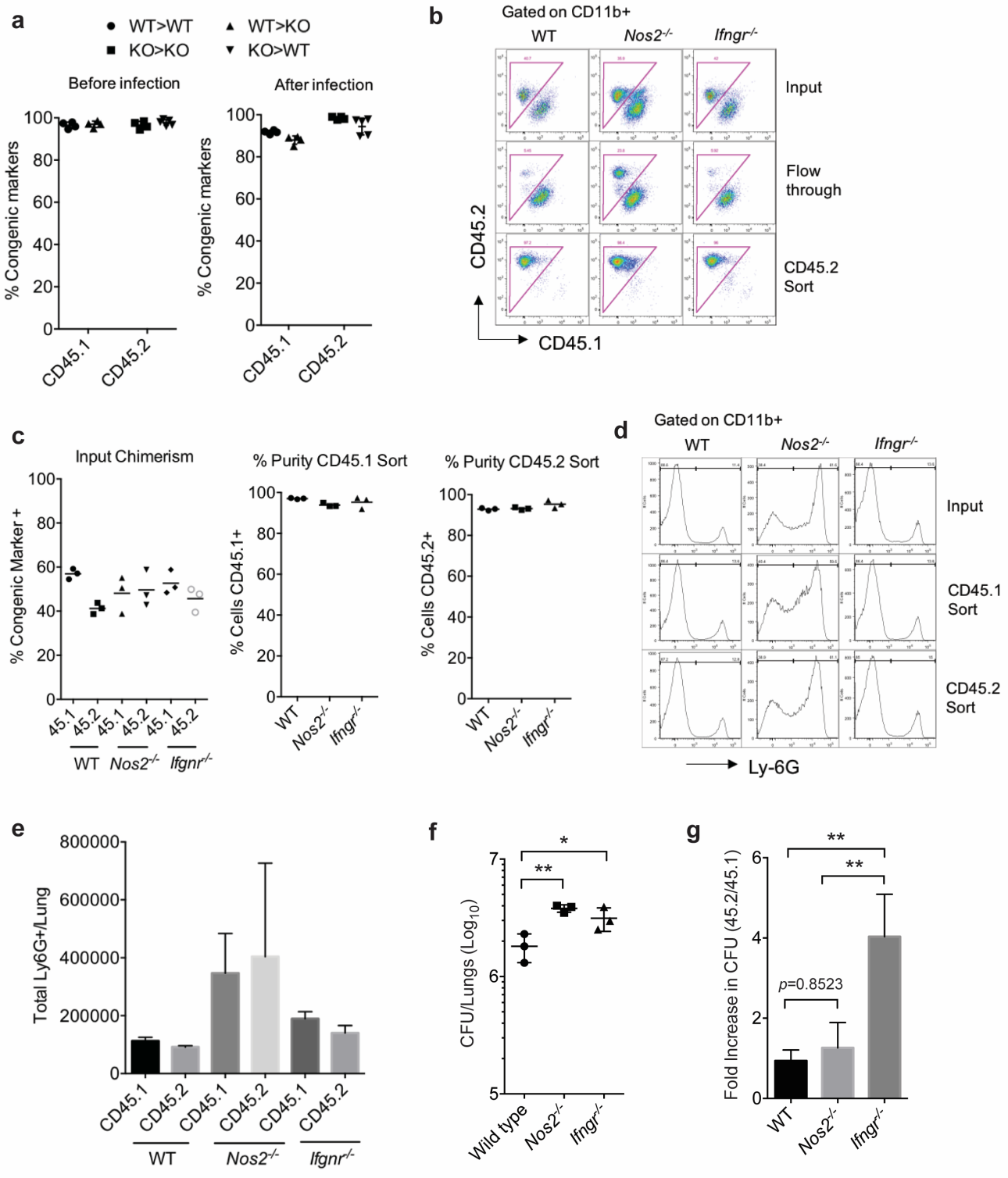

Supplementary Figure 2. Mice maintain chimerism after bone marrow reconstitution, and purified cells are representative of the total population.

Bone marrow chimeric mice from "Figure 1b" were generated by reconstituting lethally irradiated C57BL/6 (WT) and *Nos2*$^{-/-}$ mice with bone marrow cells from WT or *Nos2*$^{-/-}$ mice, and these animals were infected with Mtb. Notation indicates 'donor genotype -> recipient genotype'. **a.** Chimerism of the congenically marked CD11b+ leukocytes were determined in the blood before infection, and in the lung of each animal after infection. **b**. Purity of the cell populations depicted in "Figure 1c" were determined in the sorted and flow through fraction of MACS purification of the lung leukocytes from mixed-bone marrow chimeric mice. **c.** Relative chimerism of the congenic markers in the lung of mixed bone marrow chimeric mice before and after magnetic cell sorting. **d.** The relative proportion of CD11b+Ly-6G+ and CD11b+Ly-6G- cells was quantified throughout MACS purification. **e**. The total numbers of neutrophils (CD11b+Ly-6G+) and **f**. the absolute number of bacteria (CFU) in the lungs of bone marrow chimeric mice. **g**. Relative bacterial burden in the purified congenically marked cells of different genotypes (CFU). (**f**-**g**). Data shown (Mean ± SD) are from one experiment, that is representative of two. **, $p<0.01$, one-way ANOVA with Tukey's multiple comparison test.

Supplementary Figure 3:

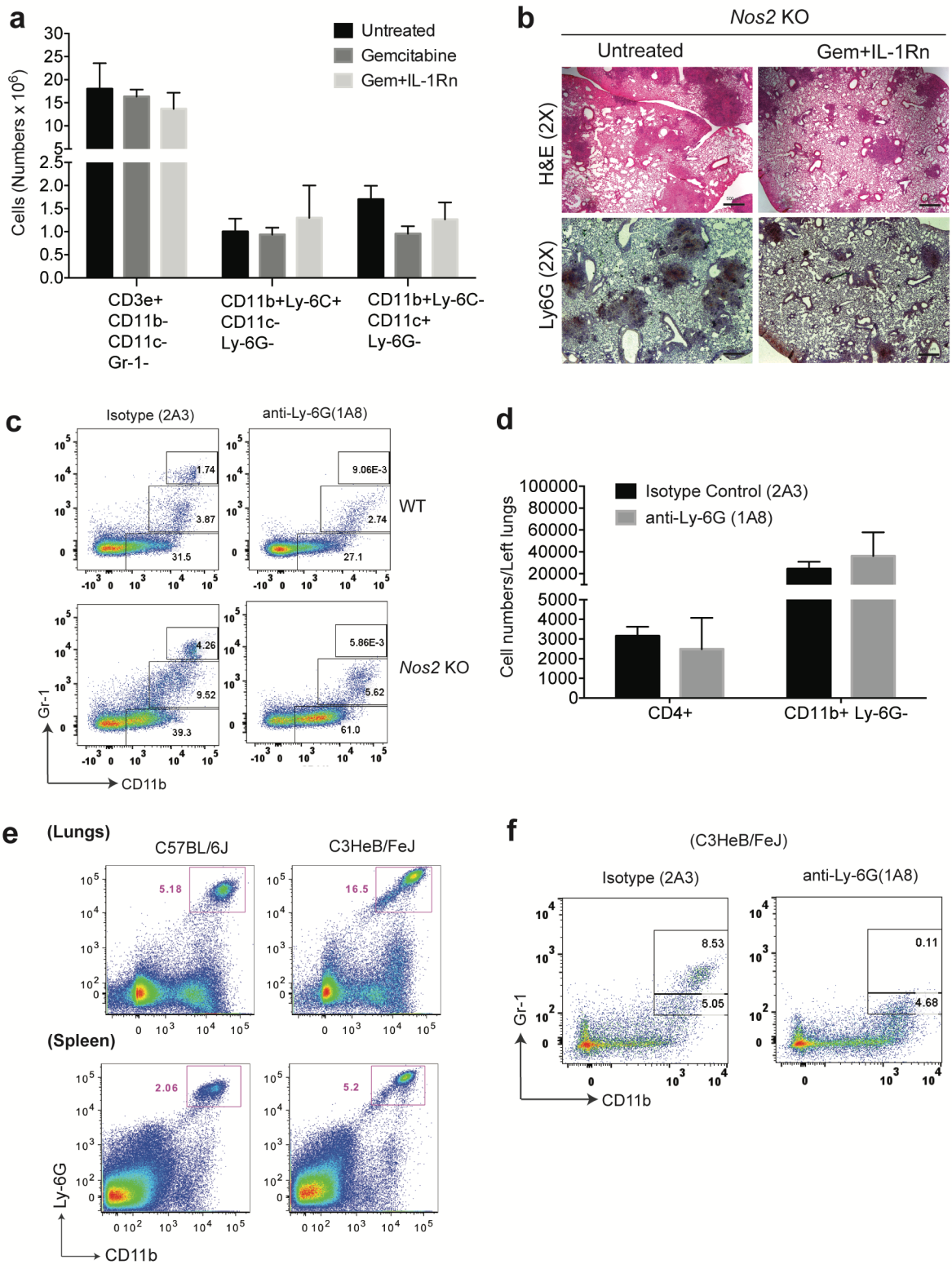

Supplementary Figure 3. Specificity of neutrophil depletion methods.

Mtb infected *Nos2*$^{-/-}$ mice were infected with Mtb, treated with gemcitabine, or gemcitabine and IL-1Rn, as shown in Fig 1. **a**. After four weeks of infection, the total number of CD3e^{+}, CD11b^{+}Ly-6C^{+}Ly-6G^{-} and CD11b+Ly-6C^{-}Ly-6G^{-} cells in the lung leukocytes were determined by flow cytometry. Data shown (Mean ± SD) are from one experiment, which is representative of two. **b**. Lung histopathology after hematoxylin/eosin staining and immunohistochemistry for Ly-6G was performed in the respective lung sections (Scale represents 500μm). **c-d.** WT and *Nos2*$^{-/-}$ mice were depleted of neutrophils by administering anti-Ly6G antibody (1A8). Control groups received isotype antibody (2A3). Effect of antibody depletion on CD11b+Gr-1^{hi} cells (**c**), and other lung leukocytes (live CD4^{+}CD11b^{+}Ly-6G^{-}) (**d**) was determined in both genotypes. Data shown in "**d**" (Mean ± SD) are from one experiment, that is representative of two. **e**. C57BL/6 and C3HeB/FeJ mice were infected with Mtb H37Rv by aerosol and five weeks after infection neutrophil infiltration into lungs and spleen was determined by flow cytometry. Representative FACS plots are shown. **f**. Neutrophil depletion in the lungs of C3HeB/FeJ mice was carried out by 1A8 administration. Control mice received the isotype-matched antibody, 2A3. Flow cytometry was performed 4 weeks after infection. Representative FACS plot demonstrate depletion of Gr-1^{high} neutrophils.

Supplementary Figure 4:

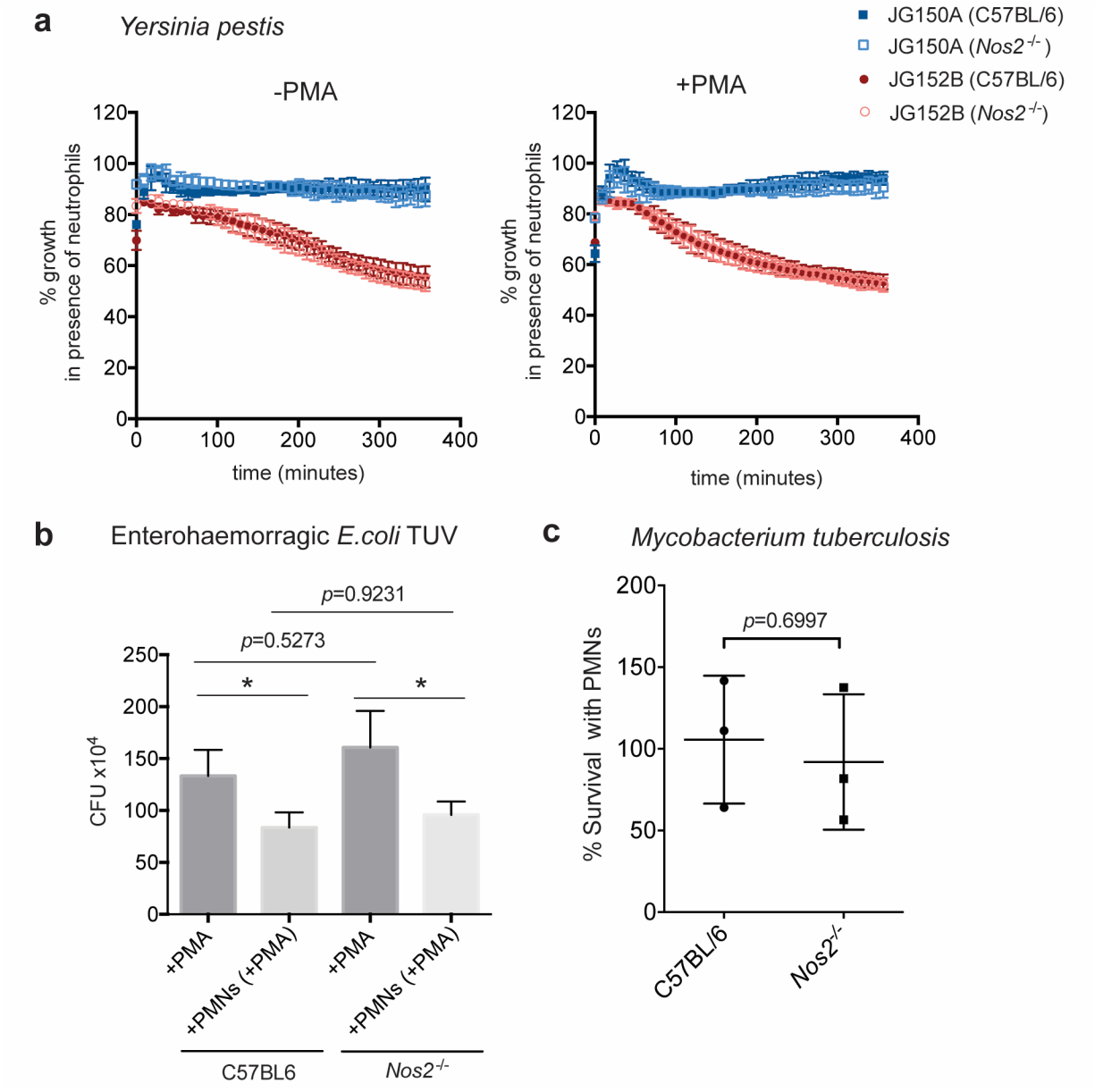

Supplementary Figure 4. Neutrophils do not kill *M. tuberculosis ex vivo*.

Neutrophils were isolated from the bone marrow of wild type C57BL6 and *Nos2*$^{-/-}$ mice. Isolated PMNs were either activated with PMA or left untreated as indicated in figure. % killing of **a**. *Yersinia pestis* and **b**. Enterohemorragic *E. coli*. TUV were measured by calculating the survival of these bacterial strains either in the presence of media or PMNs. **c.** % survival of *M. tuberculosis* Erdman was determined after 16h incubation either with media or PMNs. (**b**-**c**). Values shown (Mean ± SD), are from one experiment. **, p<0.01, one-way ANOVA with Tukey's multiple comparison test.

Supplementary Figure 5:

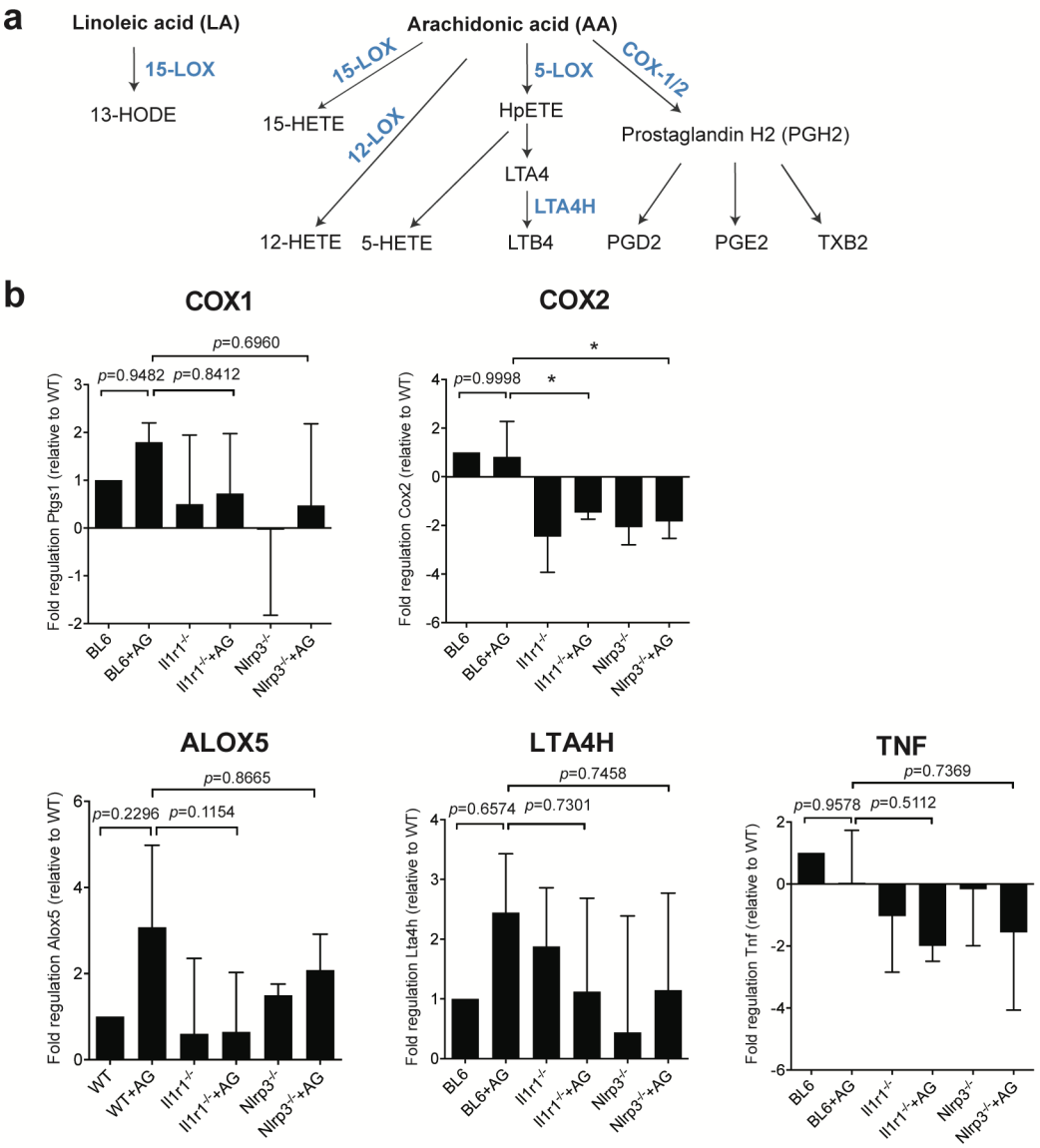

Supplementary Figure 5. Effect of Nos2 and Nlrp3 and Il1r1 inhibition on the expression of TNF and eicosanoid modifying genes.

a. Biosynthetic pathways of lipoxygenases- and cyclooxygenase-derived eicosanoids[1]. **b**. Relative mRNA abundance of eicosanoid biosynthetic enzymes and TNF in the total RNA isolated from the lungs of indicated mouse strains was determined by RT-PCR. Fold regulation of each transcript was calculated relative to the wild type. Data shown (Mean ± SD) are representative of two independent experiments, *, $p<0.05$; **, $p<0.001$, one-way ANOVA with Tukey's multiple comparison test.

Supplementary Figure 6:

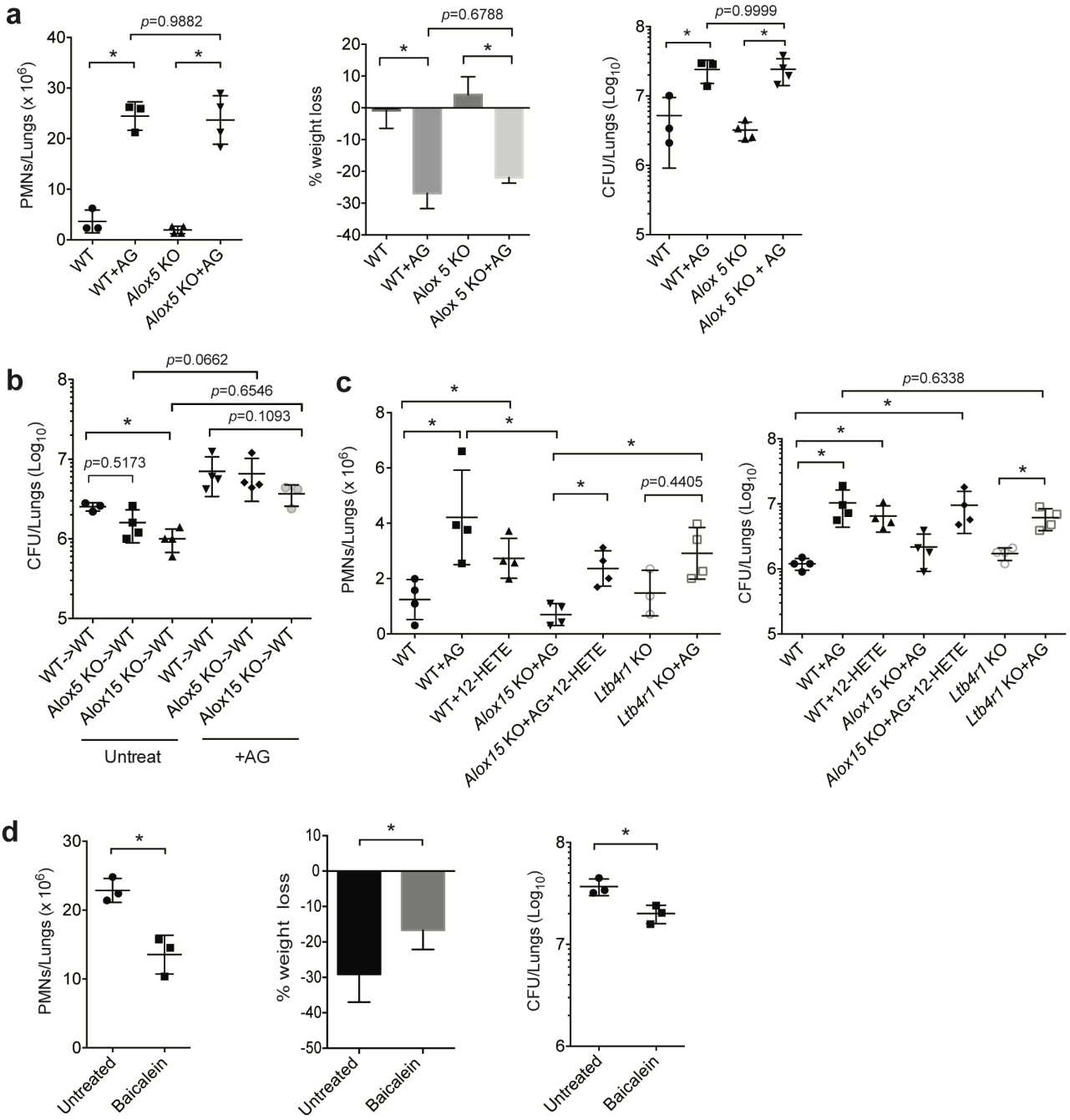

Supplementary Figure 6. 12/15-LOX has a larger effect on TB disease than 5-LOX or LTB4R1.

Wild type C57BL/6 (WT) and *Alox5*$^{-/-}$ mice were treated with Nos2 inhibitor, AG, and infected with Mtb by aerosol (~300 CFU). **a.** Neutrophil numbers in the total lung leukocytes was measured by flow cytometry, % weight loss in each cohort was calculated relative to pre-infection weight, and bacterial burden in the lung homogenates was calculated by CFU enumeration. Values shown (Mean ± SD) are from one experiment representative of two independent experiments, *, $p<0.05$; **, $p<0.001$, one-way ANOVA with Tukey's multiple comparison test. **b**. Lung bacterial burden in cohorts of the indicated bone marrow chimeric mice were determined five weeks after infection. Notation indicates bone marrow donor genotype -> recipient genotype. Aminoguanidine treated groups are indicated ("AG"). Values shown (Mean ± SD) are from one experiment, *, $p<0.05$; **, $p<0.001$, one-way ANOVA with Tukey's multiple comparison test. **c**. WT, *Alox15*$^{-/-}$, *Ltb4r1*$^{-/-}$ were treated with AG and infected with Mtb. As indicated, cohorts of mice were left untreated. At one day post infection, 12-HETE was administered to the indicated cohorts via osmotic mini-pumps until the termination of the experiment. Neutrophil infiltration to the lungs was measured by flow cytometry and bacterial burden in the lungs of each study group was measured by CFU enumeration. Values shown (Mean ± SD) are from one experiment, *, $p<0.05$; **, $p<0.001$, one-way ANOVA with Tukey's multiple comparison test. **d**. Mtb infected *Nos2*$^{-/-}$ mice were treated with the 12/15-LOX inhibitor, baicalein, by subcutaneous implantation of mini-osmotic pumps. 'Untreated' groups were treated with propylene glycol as vehicle control. Neutrophil infiltration to the lungs, % weight loss, and CFU in the lung homogenates were assessed. Values shown (Mean ± SD) are representative of two independent experiments. *, $p<0.05$, Two-tailed unpaired *t*-test with Welch correction.

Supplementary Figure 7:

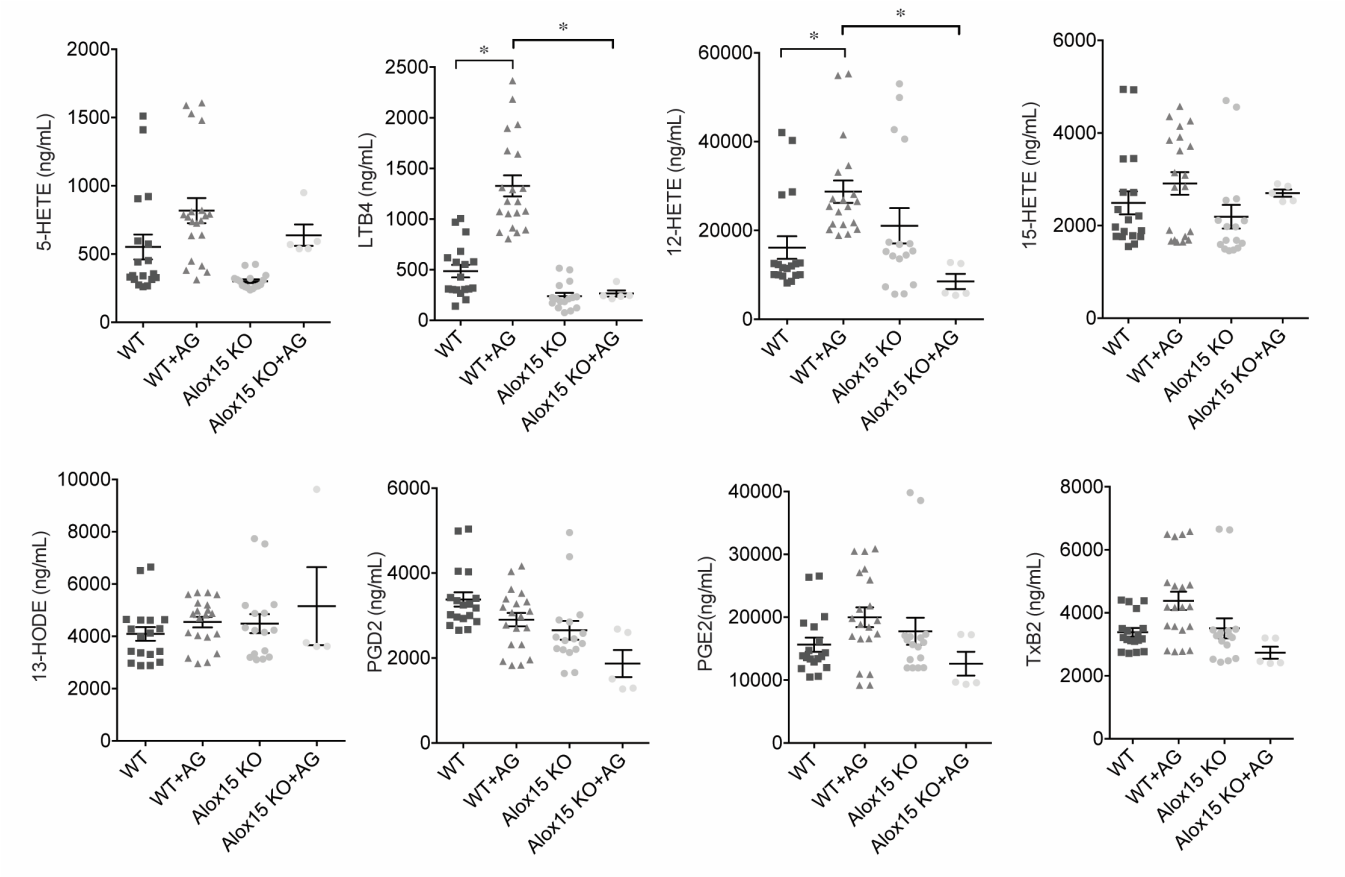

Supplementary Figure 7. 5- and 12/15-Lipoxygenase products in the lung correlate with the extent of inflammation.

Wild type C57BL/6 (WT) and *Alox15*$^{-/-}$ mice were treated with Nos2 inhibitor, AG, and infected with Mtb. Four wks post-infection, abundance of indicated eicosanoids in the lung homogenates were measured by LC-MS. 5-lipoxygenase derived 5-hydroxyeicosateraenoic acid (5-HETE) and leukotriene B4 (LTB4), 12/15-lipoxygenase derived 12-Hydroxyeicosatetraenoic acid (12-HETE), 15-hydroxyeicosateraenoic acid (15-HETE), and 13-hydroxy octadecadienoic acid (13-HODE), and cyclooxygenase derived prostaglandin D2 (PGD2), prostaglandin E2 (PGE2) and thromboxane (TxB2) were measured. Values shown (Mean ± SEM), *, $p<0.05$, Two-tailed paired *t*-test. Data are from one experiment representative of two.

Supplementary Figure 8:

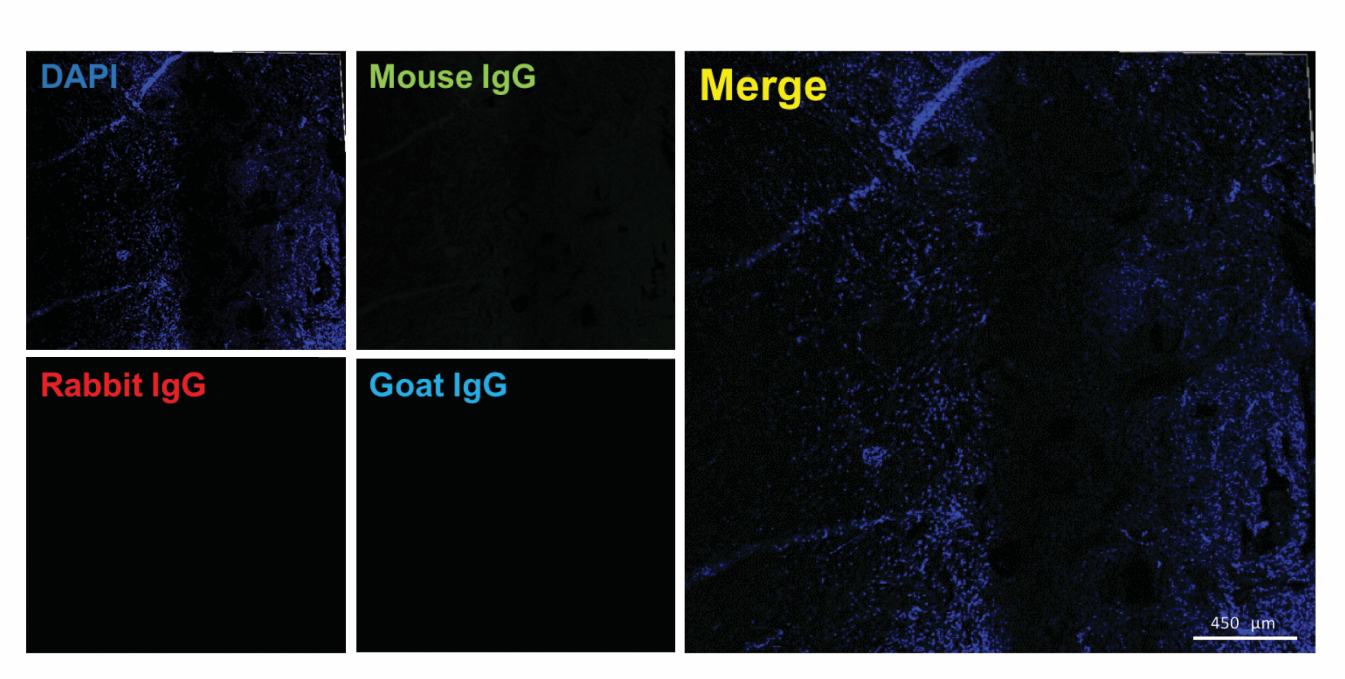

Supplementary Figure 8. Nonspecific antibodies do not stain human lung sections.
Isotype matched antibodies are used as negative controls for immunohistochemical staining of human lung sections (Scale represents 450μm).

Supplementary Figure 9:

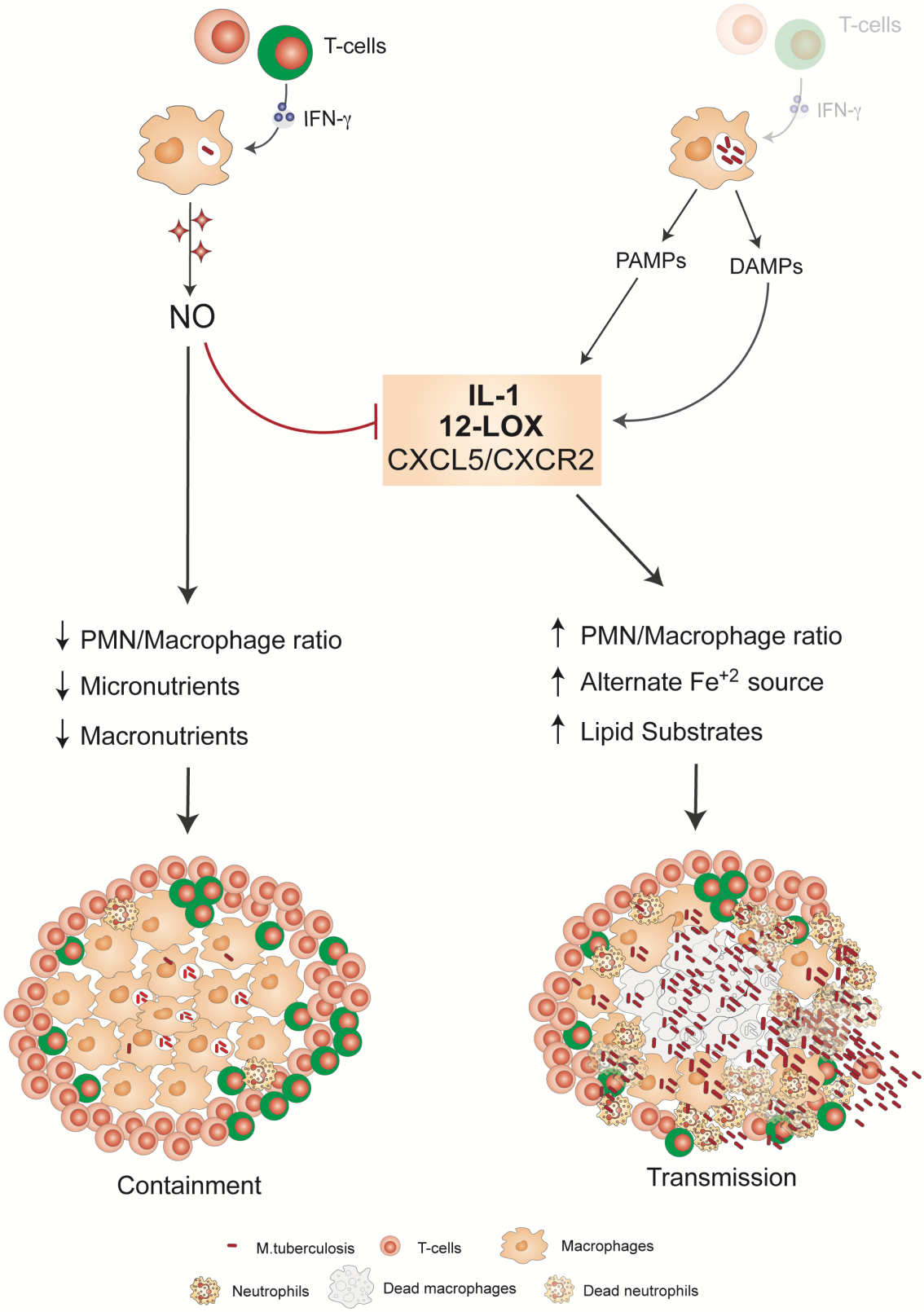

Supplementary Figure 9. Model to describe the role of pro- and anti-inflammatory pathways in TB pathogenesis.

Mtb infection promotes IL-1 mediated inflammatory responses through the production of both 'pathogen" and 'damage-associated molecular patterns ('PAMP' and 'DAMP'). Unchecked, persistent IL-1 production acts in concert with 12/15-LOX products and CXCR2 signaling to promote neutrophil influx to the site of infection (right of figure). In resistant individuals (Left of figure) T cell-derived IFN-γ induces the production of nitric oxide (NO) from myeloid cells. This mediator protects the host largely by repressing persistent IL-1 production and preventing uncontrolled neutrophil recruitment. Genetic polymorphisms, such as promoter mutations in IL1B[2] or ALOX12 (this study) can influence the balance between pro- and anti-inflammatory mediators. The local balance between these pathways determines the environment in which the pathogen resides. At sites of high neutrophil/macrophage ratio, tissue integrity is compromised, and bacteria replicate relatively rapidly, due to the availability of micro- and macro-nutrients. This model predicts that Mtb has adapted to replicate exuberantly at sites of inflammatory tissue damage that promote transmission of the pathogen.

Supplementary Table 1. Genome-wide fitness profiling of Mtb mutants in C57BL/6, C3HeB, and NOS2-deficient mice. (Supplied as a separate Excel file)

Supplementary Table 2. Mutants with significantly altered in C3HeB and Nos2 KO mice compared to C57BL/6 mice. (Supplied as a separate Excel file)

Supplementary Table 3: Polymorphisms used for genotyping human cohorts. (Supplied as a separate Excel file)

Supplementary Table 4. Single nucleotide polymorphisms significantly associated with tuberculosis susceptibility.

Gene	SNP ID	Trait	No.	Allele (frequency%)		Genotype			Allelic comparison				
				A	a	AA	Aa	aa	χ^2	*P* *	*P adj* #	OR	95%CI
LTA4H	rs2660898 T>G	TB	943	1078(57.2)	808(42.8)	301	476	166					
		HC	934	1137(60.9)	731(39.1)	331	475	128	5.34	0.021	0.48	1.16	1.023-1.328
	rs17525495 T>C	TB	943	1273(67.5)	613(32.5)	439	395	109					
		HC	934	1330(71.2)	538(28.8)	452	426	56	6.05	0.014	0.29	1.19	1.036-1.368
5-LOX	rs4986832 G>A	TB	943	1582(83.9)	304(16.1)	677	228	38					
		HC	934	1496(80.1)	372(19.9)	621	254	59	9.16	0.0025	0.03	0.773	0.654-0.914
	rs6413416 G>A	TB	943	1505(79.8)	381(20.2)	618	269	56					
		HC	934	1557(83.4)	311(16.6)	649	259	26	7.88	0.005	0.06	1.267	1.074-1.496
COX-1	rs1330344 G>A	TB	943	1030(54.6)	856(45.4)	290	450	203					
		HC	934	1093(58.5)	775(41.5)	311	471	152	5.81	0.016	0.32	1.172	1.030-1.334
12-LOX	rs9904779 C>G	TB	943	961(51.0)	925(49.0)	258	445	240					
		HC	934	856(45.8)	1012(54.2)	212	432	290	9.89	0.0017	0.027	0.814	0.716-0.925
	rs3840880 DEL>G	TB	943	1027(54.5)	859(45.5)	301	425	217					
		HC	934	1119(59.9)	749(40.1)	346	427	161	11.38	0.0007	0.01	1.250	1.098-1.422

Supplementary Table 5. Deuterium-labeled or unlabeled internal standard used for LC-MS based quantification of eicosanoids

.

Compound	Start Time (min)	End Time (min)	Precursor (m/z)	Product (m/z)	Collision Energy (V)	RF Lens (V)
LTB4	**0**	**10**	**335.2**	**194.9**	**17**	**71**
LTB4	0	10	335.2	316.9	15	71
LTB4-d4	**0**	**10**	**339.2**	**197.1**	**17**	**66**
LTB4-d4	0	10	339.2	321.2	16	66
LXA4	**0**	**10**	**351.2**	**115.2**	**13**	**56**
LXA4	0	10	351.2	217.4	21	56
LXA4	0	10	351.2	271	17	56
LXA4-d4	**0**	**10**	**356.2**	**115.2**	**13**	**58**
LXA4-d4	0	10	356.2	221.97	21	58
PGE2, PGD2	**0**	**10**	**351.2**	**271.3**	**18**	**52**
PGE2, PGD2	0	10	351.2	315	13	52
PGE2-d9	**0**	**10**	**360.2**	**280.2**	**19**	**55**
PGD2-d4	**0**	**10**	**355.2**	**275.1**	**19**	**49**
TXB2	**0**	**10**	**369.2**	**195.2**	**13**	**53**
TxB2	0	10	369.2	168.9	18	53
TXB2-d4	**0**	**10**	**373.3**	**199.2**	**13**	**51**
TXB2-d4	0	10	373.3	172.9	19	51
13-HODE	**10**	**15**	**295.2**	**171.1**	**18**	**64**
13-HODE-d4	**10**	**15**	**299.2**	**172.1**	**18**	**64**
5-HETE	**10**	**15**	**319.1**	**115**	**15**	**73**
5-HETE-d8	**10**	**15**	**327.3**	**116.1**	**15**	**75**
12-HETE	**10**	**15**	**319.1**	**208**	**13**	**76**
12-HETE-d8	**10**	**15**	**327.3**	**214.1**	**14**	**75**
12-HETE-d8	10	15	327.3	184.2	15	75
15-HETE	**10**	**15**	**319.1**	**219**	**13**	**75**
15-HETE-d8	**10**	**15**	**327.3**	**226.2**	**13**	**76**
HETE's	10	15	327.3	59.1	24	75
HETE's	10	15	319.1	257.1	15	74
HETE's	10	15	319.1	301.2	11	74
HETE's-d8	10	15	327.3	265.2	15	75
HETE's-d8	10	15	327.3	309.1	12	75

Supplementary References

1. Dennis, E. A. & Norris, P. C. Eicosanoid storm in infection and inflammation. *Nat. Rev. Immunol.* **15,** 511–523 (2015).
2. Zhang, G. *et al.* Allele-specific induction of IL-1β expression by C/EBPβ and PU.1 contributes to increased tuberculosis susceptibility. *PLoS Pathog.* **10,** e1004426 (2014).